Japanese Journal of Applied Physics

The Japan Society of Applied Physics

RAPID COMMUNICATION

High thermal performance hybrid GaInAsP/SOI ridge waveguide lasers with enhanced heat dissipation structure

To cite this article: Moataz Eissa *et al* 2023 *Jpn. J. Appl. Phys.* **62** 010905

View the article online for updates and enhancements.

You may also like

- Voltage reduction of 808 nm GaAsP/(Al)GaInP laser diodes with GaInAsP intermediate layer
Zhen Zhu, , Xin Zhang et al.
- InP membrane integrated photonics research
Yuqing Jiao, Nobuhiko Nishiyama, Jos van der Tol et al.
- A design analysis of a GaInP/GaInAs/GaAs-based 980 nm Al-free pump laser using self-consistent numerical simulation
Muhammad Nawaz and Komet Permthammasin

This content was downloaded from IP address 131.112.125.219 on 27/09/2024 at 06:34

Japanese Journal of Applied Physics **62**, 010905 (2023)
https://doi.org/10.35848/1347-4065/acacdb

RAPID COMMUNICATION

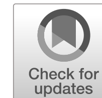

High thermal performance hybrid GaInAsP/SOI ridge waveguide lasers with enhanced heat dissipation structure

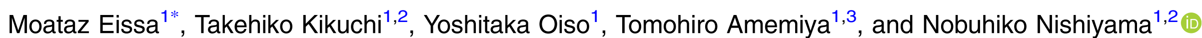

Moataz Eissa[1*], Takehiko Kikuchi[1,2], Yoshitaka Oiso[1], Tomohiro Amemiya[1,3], and Nobuhiko Nishiyama[1,2]

[1]*Department of Electrical and Electronic Engineering, Tokyo Institute of Technology, 2-12-1, O-okayama, Meguro-ku, Tokyo 152-8550, Japan*
[2]*Photonics Electronics Technology Research Association (PETRA), 1-20-10, Sekiguchi, Bunkyo-ku, Tokyo 112-0014, Japan*
[3]*Institute of Innovative Research (IIR), Tokyo Institute of Technology, 2-12-1, O-okayama, Meguro-ku, Tokyo 152-8550, Japan*

[*]E-mail: eissa.m.aa@m.titech.ac.jp

Received October 7, 2022; revised November 24, 2022; accepted December 18, 2022; published online January 6, 2023

Hybrid GaInAsP/SOI ridge waveguide Fabry–Pérot lasers with reduced thermal resistance were fabricated and measured. The lasers were formed by room-temperature surface-activated bonding of InP and silicon-on-insulator wafers. Thin SiO_2 film was introduced as ridge-sidewall insulation to increase heat flow to the p-electrode side-metal. By incorporating a thermal shunt structure and Au electroplating, a single-facet output power of 20 mW and lasing operation up to 110 °C were achieved for a cavity length of 2.0 mm under continuous-wave conditions. The proposed structure showed low thermal resistance of 14.3 K W^{-1} and a threshold current density of approximately 0.7 kA cm^{-2}.
© 2023 The Japan Society of Applied Physics

Photonic integrated circuits (PICs) with heterogeneous integration technology have been a field of intense research in silicon photonics.[1–3] Their potential to introduce different material technologies to commercial silicon chips opens the path for large-scale integration of high performance PICs with various optical functionalities, which are challenging to achieve using conventional silicon-on-insulator (SOI) platforms.[4–6] In particular, the heterogeneous integration of hybrid III–V/SOI lasers by direct bonding provides an appropriate solution for on-chip light sources for telecommunication and datacenter applications operating near 1.3 and 1.55 μm wavelength ranges.[2,7] This integration of lasers within the SOI circuitry has enabled realization of wavelength-tunable external-cavity structures operating effectively across the entire wavelength band by using distributed Bragg reflector, ring resonator and loop mirror devices.[8–12] Moreover, hybrid III–V/SOI ring lasers have also been reported, in which the light was coupled from the III–V/SOI ring laser to the Si bus-waveguide by a directional coupler.[13–16]

Despite their advantages, hybrid III–V/SOI lasers exhibit relatively high thermal resistance values due to the poor thermal conductivity of the buried-oxide layer in SOI substrates.[17] Although the buried-oxide layer is required as optical cladding, its thermal insulation characteristics hinder heat sinking from the laser core to the Si substrate, lowering the output power with reduced energy efficiency under continuous-wave (CW) conditions, especially at elevated temperatures.[18,19] Various approaches have been adopted to reduce the thermal resistance of hybrid III–V/SOI lasers. For example, relatively wide III–V mesa structures with a thick p-electrode metal were used to absorb and spread the generated heat away from the laser core. Proton (H^+) implantation or III–V layer oxidation was adopted for current confinement in such structures.[20,21] In contrast, another method is implementing a thermal shunt structure connecting the laser core to the Si substrate through a short path with high thermal conductivity. Hybrid III–V/SOI lasers with metal and polysilicon thermal shunt materials have been investigated in the literature. Although sub-milliwatt output power levels have been reported with metal thermal shunt structures,[22,23] higher output power levels up to 30 mW were reported for wide-mesa structures with H^+ current confinement and polysilicon thermal shunts.[24] However, a relatively high threshold current density of ~1.8 kA cm^{-2} was demonstrated for the latter structure.

This letter reports the fabrication and measurement of high thermal performance hybrid GaInAsP/SOI ridge waveguide Fabry–Pérot (FP) lasers with reduced thermal resistance. The bonding process was previously reported.[25,26] Moreover, the laser structure relied on a 3.5 μm wide III–VIII–V ridge waveguide with a 0.5 μm wide Si waveguide underneath, attached to a highly conductive thermal path to the Si substrate for reduction of thermal resistance. As a result, a single-facet output power of 20 mW and lasing operation up to 110 °C were achieved under CW conditions for a 2.0 mm cavity length. In addition, a thermal resistance of ~14.3 K W^{-1} and a threshold current density of ~0.7 kA cm^{-2} were demonstrated.

First, we designed a structure that improves heat dissipation from the III–V ridge waveguide. In conventional monolithic ridge waveguide lasers, the ridge waveguide structure is covered by a sufficiently thick SiO_2 layer acting as horizontal optical cladding for the transverse mode in addition to its electrical insulation characteristics. However, for hybrid III–V/SOI lasers with external-cavity structures, the SiO_2 layer also acts as vertical cladding for the external Si waveguide with metal microheaters.[26] Figures 1(a) and 1(b) show the calculated optical intensity of the fundamental TE mode using the finite difference method (FDM) at the III–V/SOI gain section with conventional ridge insulation and an external Si waveguide section, respectively. The SiO_2 cladding layer was characterized by a horizontal cladding height (h_y) and vertical cladding thickness (w_x), as both thicknesses were naturally coupled during plasma-enhanced chemical vapor deposition. We assumed in the calculation that $w_x = ½h_y$ to compare the performance with the improved structure described below, which is a valid approximation in most cases with deposition rate anisotropy. Figure 1(c) shows optical absorption losses for both sections due to the proximity of the p-electrode and microheater metals and the estimated laser thermal resistance. Thermal resistance values were estimated by commercial software providing a heat transfer simulation model using a two-dimensional finite-element method (2D FEM). The calculation assumed the incorporation of thermal shunt and plating structures, as

 © 2023 The Japan Society of Applied Physics

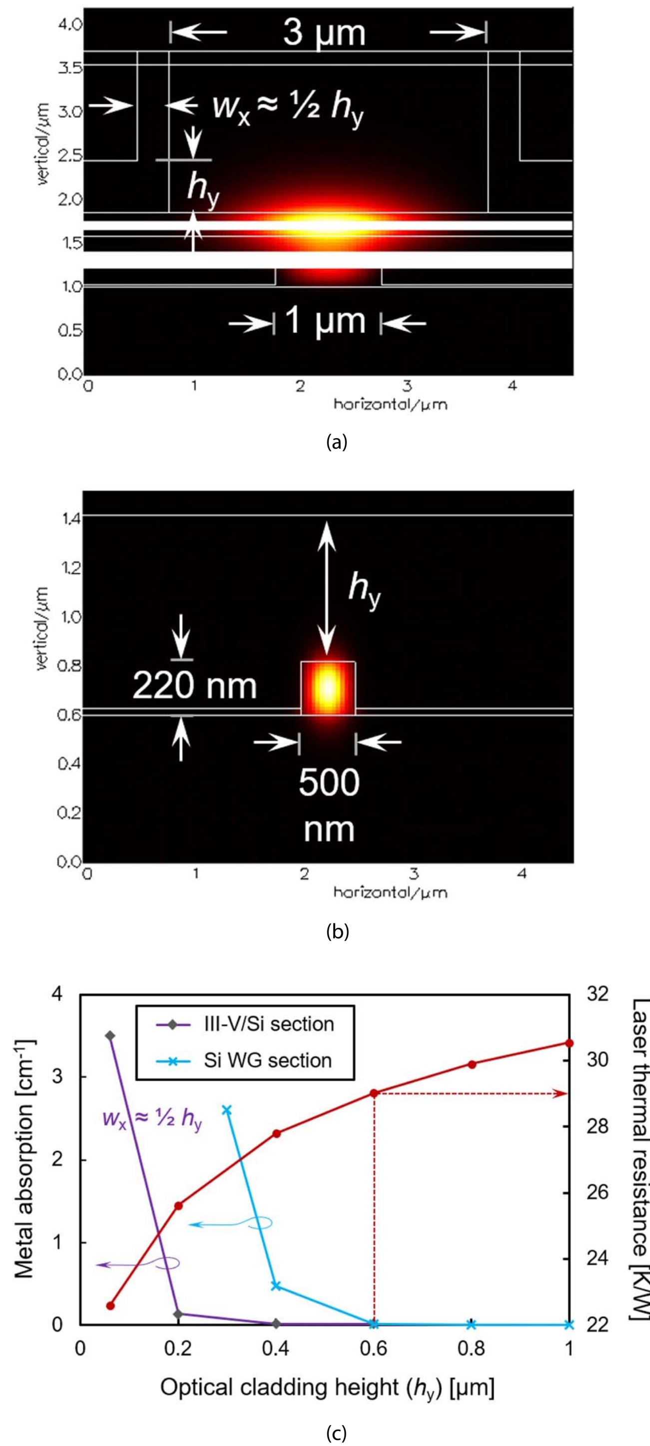

Fig. 1. (Color online) Calculated optical intensity of the fundamental TE mode at (a) the III–V/SOI gain section with conventional ridge insulation and (b) the external Si waveguide section, with (c) trade-off calculations between the metal absorption losses and the laser thermal resistance.

shown in Fig. 5(b), and a cavity length of 1.0 mm. The trade-off between metal absorption losses and laser thermal resistance was evident. Thus, the minimum possible thermal resistance was decided by the minimum horizontal cladding height ($h_y \approx 0.6\,\mu$m), at which negligible metal absorption losses could be achieved in both sections.

Although this conventional ridge insulation was used in a previous report,[26] we further improved the insulation structure in this study to reduce the thermal resistance. Figure 1(c) shows that the external Si waveguide microheater dominates the metal absorption for the same cladding height. This result indicates that the vertical cladding thickness can be independently reduced while fixing the horizontal cladding height at its minimum for negligible optical losses. The decoupling of horizontal and vertical cladding thicknesses in the III–V/SOI gain section allows reduction of thermal resistance using thinner vertical cladding. Figure 2 shows a cross-sectional schematic image of the proposed hybrid GaInAsP/SOI ridge waveguide with decoupled cladding thicknesses in the horizontal and vertical directions. This improved ridge insulation structure was fabricated in two steps: the first step forms the horizontal cladding, while the second forms

 © 2023 The Japan Society of Applied Physics

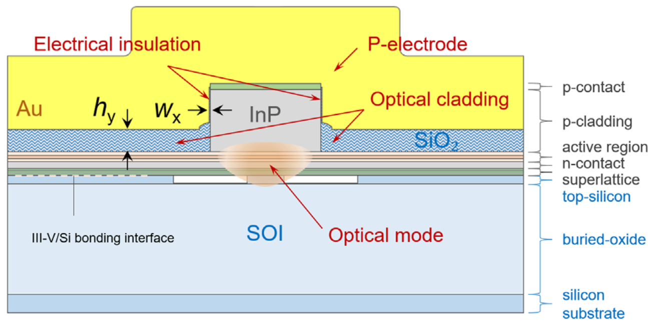

Fig. 2. (Color online) Cross-sectional schematic image of the hybrid GaInAsP/SOI ridge waveguide with decoupled ridge insulation film thicknesses in horizontal and vertical directions.

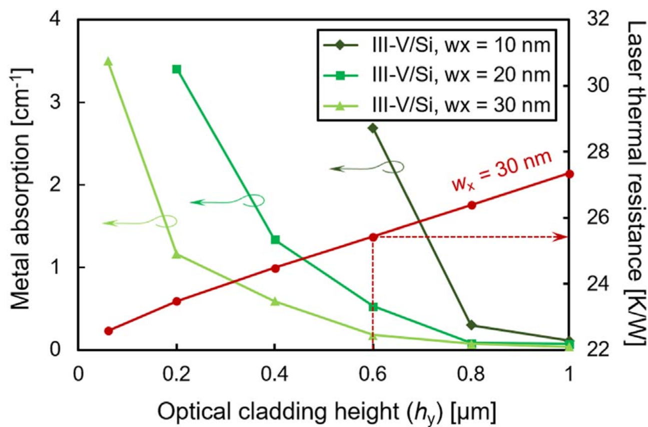

Fig 3. (Color online) Trade-off calculations between the metal absorption losses and the laser thermal resistance with improved ridge insulation.

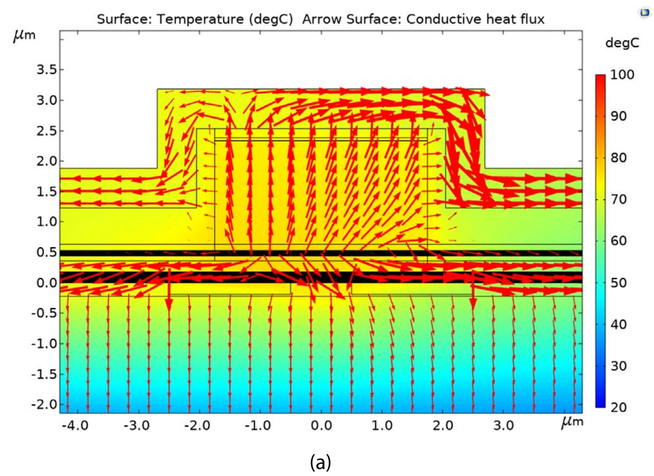

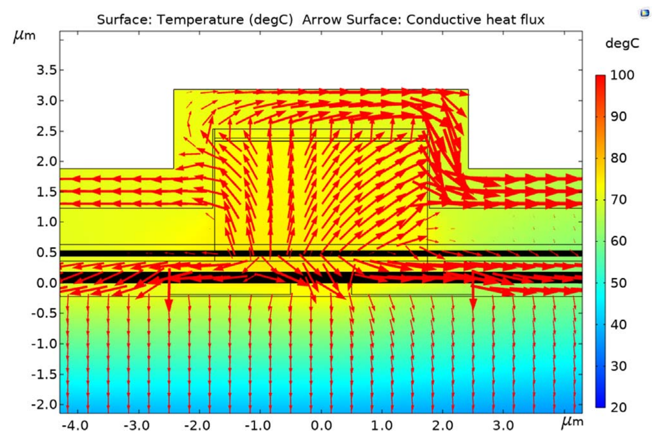

Fig. 4. (Color online) Estimated temperature distribution and heat flow (2D) within the hybrid GaInAsP/SOI ridge waveguide laser cross-section with (a) conventional and (b) improved ridge insulation.

the vertical cladding with a p-contact window opening for metallization. In particular, window opening processes usually depend on ridge dimensions and process parameters, such as the relationship between the ridge width and the lithography critical dimension (CD). For example, the conventional aligned lithography process can be easily applied for relatively wide ridges;[27,28] however, self-aligned processes are more convenient for narrow ridges with relatively high aspect ratios.[29,30] In this study, self-aligned lithography was adopted for window opening to maximize the contact area of the p-electrode and hence minimize p-contact resistance and increase heat flow.

Figure 3 shows the trade-off between the metal absorption losses for several vertical cladding thicknesses ($w_x = 10$, 20 and 30 nm) and the estimated laser thermal resistance with improved ridge insulation ($w_x = 30$ nm). The calculation assumed the incorporation of thermal shunt and plating structures, as shown in Fig. 5(b), and a cavity length of 1.0 mm. The results suggest minimum values of $h_y \approx 0.6\ \mu$m and $w_x \approx 30$ nm. In this case, metal absorption is as low as 0.18 cm^{-1}, which is almost negligible compared with the intrinsic internal loss of the laser cavity. The reduction in the value of w_x is also proportional to the reduction in thermal resistance. Moreover, heat flow profiles were calculated for the conventional and improved insulation structures to discuss such reduction qualitatively. Measurement of laser diode differential resistances at different III–V ridge widths for the 3.5 μm wide ridge suggested p-cladding and n-contact layer resistances of ~3 Ω for each. Thus, the estimated resistive heating and diode-drop heating were included in a 2D FEM heat transfer simulation model with the previously mentioned structural dimensions. The model assumed an input power of 1 W, an ambient temperature of 20 °C and a third-dimension value of 1.0 mm. Furthermore, the model considered natural air cooling from the laser top with convection heat transfer coefficient $h = 10$ W m^{-2} K^{-1}. Figures 4(a) and 4(b) show the estimated temperature distribution and heat flow within the hybrid GaInAsP/SOI ridge waveguide laser cross-section for the conventional and improved ridge insulation structures, respectively. The figure clearly shows that a lower temperature is obtained for the improved ridge insulation structure, as the heat penetrates the thin vertical cladding to be absorbed by the p-electrode side-metal, spreading away from the laser core. Note that the n-electrode exists on the left side; hence, more heat flow is directed to the right side with lower temperature. The estimated thermal resistances were 53.4 K W^{-1} and 49.6 K W^{-1} for the conventional and improved ridge insulation structures, respectively. These results correspond to a simulated reduction in thermal resistance of 9.3%. Note that thermal shunt and Au electroplating structures were not

 © 2023 The Japan Society of Applied Physics

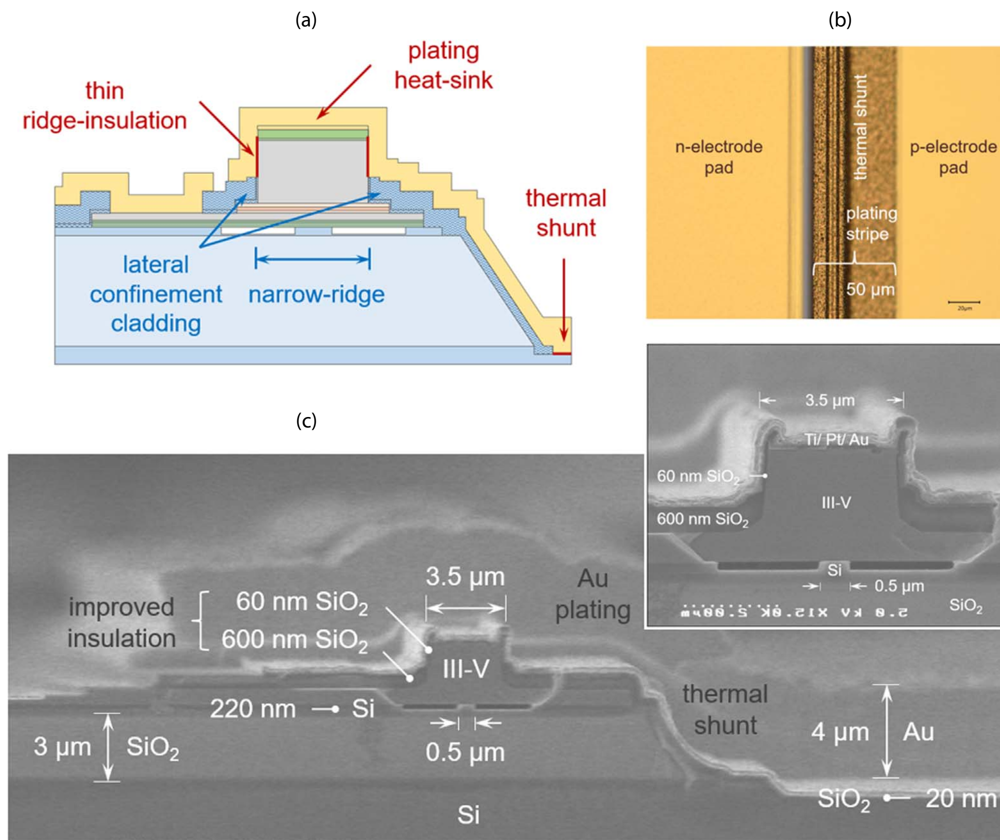

Fig. 5. (Color online) (a) Cross-sectional schematic, (b) microscopic top view and (c) cross-sectional scanning electron microscope image of the hybrid GaInAsP/SOI ridge waveguide laser with improved ridge insulation, metal thermal shunt and electroplating heat sinking structures.

included in these simulations so as to clearly characterize the effect of the proposed structure. Thus, the estimated thermal resistances are higher than those shown in Figs. 1(c) and 3, which include the effect of a thermal shunt structure and Au electroplating. For the actual devices, the thermal resistances ($Z_T = dT/dP$) were extracted from wavelength dependence on temperature ($d\lambda/dT$) and wavelength dependence on injected power ($d\lambda/dP$) through the equation $dT/dP = (d\lambda/dP)/(d\lambda/dT)$.[31] The extracted thermal resistances from FP lasers with cleaved facets were 60.6 K W^{-1} and 50.4 K W^{-1} for the conventional and improved ridge insulation structures, respectively. These results correspond to an experimental reduction in thermal resistance of 16.8%.

Although the improved ridge insulation structure achieves a reduction in thermal resistance, further reduction is possible by introducing a highly conductive thermal shunt structure connecting the laser core directly to the Si substrate to boost the heat sinking effect. This path starts with the improved ridge insulation structure with thin vertical cladding, penetrates the SOI buried-oxide through the p-electrode metal, as a thermal shunt structure with a thick Au layer formed by electroplating, and ends with a SiO_2 thin film in direct contact with the Si substrate. This structure enhances heat dissipation from the laser core; hence, a much lower thermal resistance can be obtained. Although the path is designed for maximum heat flow, SiO_2 thin films are required for optical cladding and electrical insulation of the III–V ridge and Si substrate, respectively. Figure 5(a) shows a schematic of the hybrid GaInAsP/SOI ridge waveguide laser with improved ridge insulation, metal thermal shunt and electroplating heat sinking structures.

Hybrid GaInAsP/SOI ridge waveguide FP lasers were fabricated with the previously mentioned heat dissipation structure for experimental demonstration. First, room-temperature surface-activated bonding (SAB) was performed using fast atom beam irradiation for a patterned 220-nm thick SOI wafer with Si waveguides of width 0.5 μm[32] and an unpatterned GaInAsP/InP multiple quantum well epitaxial wafer. The active region comprises five quantum well layers (6 nm each) with $Ga_{0.22}In_{0.78}As_{0.81}P_{0.15}$ material under 1.10% compressive strain and six barrier layers (10 nm each) with $Ga_{0.25}In_{0.75}As_{0.50}P_{0.50}$ under 0.15% tensile strain for light emission around a wavelength of 1.55 μm. Subsequently, the 3.5 μm wide III–V ridge was processed through electron beam lithography to accurately align the ridge waveguide section to the Si waveguide. The 3 μm thick buried-oxide was etched before introducing the improved ridge insulation. The horizontal optical cladding layer was introduced to the ridge waveguide by depositing a thick SiO_2 film ($h_y = 0.6$ μm) followed by wet and dry etching processes to remove the accompanying SiO_2 films deposited on the ridge-sidewalls by process anisotropy and on the exposed Si substrate surface, respectively. Note that the wet etching process was performed through a lithography-defined window by a buffered hydrofluoric etchant with a slow etching rate to accurately control the etching depth. Then, a thin SiO_2 film (w_x = 60 nm) was deposited on top of the remaining horizontal cladding. The deposition process was

 © 2023 The Japan Society of Applied Physics

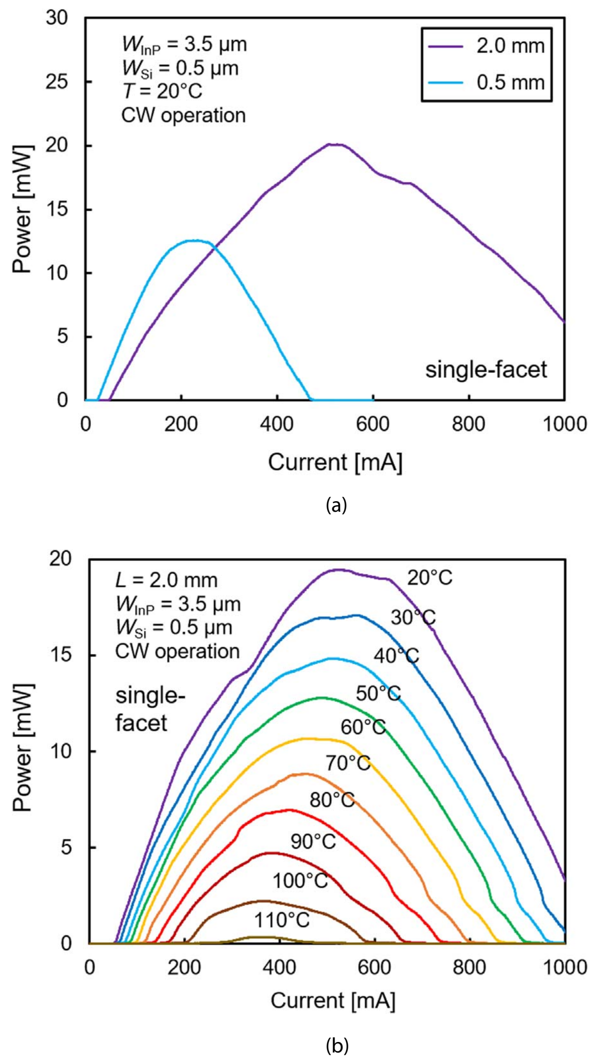

Fig. 6. (Color online) Light output characteristics of hybrid GaInAsP/SOI FP ridge waveguide lasers with (a) different cavity lengths and (b) various stage temperatures.

performed in two steps to maintain a 20-nm thin SiO_2 film on the Si substrate surface by etching the SiO_2 layer deposited in the first step. After that, the n-contact window (single-sided) was opened by conventional photolithography, while the p-contact window was opened by self-aligned lithography due to CD limitations. The process complexity was reduced by depositing p- and n-electrode metals simultaneously using an electron-gun evaporator with a Ti/Pt/Au layer stack of thicknesses 50 nm/20 nm/600 nm, respectively. Finally, a 4-μm thick Au electroplating stripe with a width of 50 μm was introduced to the p-electrode metal to cover the high-temperature-gradient area in order to improve heat spreading and increase the conductivity of the thermal shunt structure. Figure 5(b) shows a microscopic top view of the thermal shunt structure with an Au electroplating stripe for the fabricated hybrid GaInAsP/SOI ridge waveguide laser. Finally, FP lasers were formed by facet cleavage with cavity lengths of 0.5 mm and 2.0 mm. Figure 5(c) shows a cross-sectional scanning electron microscope image of the fabricated hybrid lasers with cleaved facets.

Figure 6(a) shows light output versus current (*I*–*L*) characteristics of the hybrid GaInAsP/SOI ridge waveguide FP lasers fabricated with the previously mentioned structural conditions at different cavity lengths. Measurements were performed under CW operation at a stage temperature of 20 °C. Threshold currents for the cavity lengths of 0.5 mm and 2.0 mm were 18 mA and 48 mA, corresponding to threshold current densities of ~1.0 kA cm^{-2} and ~0.7 kA cm^{-2}, respectively. Single-facet slope efficiencies of 0.096 W A^{-1} and 0.067 W A^{-1} were achieved for the 0.5 mm and 2.0 mm cavities with saturated output power values of 12.5 mW and 20.0 mW, respectively. Note that the total output power is double the presented values due to cavity symmetry. These results are attributed to the strong current confinement provided by the ridge waveguide structure and the enhanced heat dissipation structure incorporating improved ridge insulation, metal thermal shunt and Au electroplating.

Furthermore, the characteristic temperature of the threshold current (T_0), the characteristic temperature of the external differential quantum efficiency (T_1) and the thermal resistance (Z_T) were extracted from the *I*–*L* characteristics at higher temperatures to evaluate the thermal performance of the lasers experimentally. Figure 6(b) shows the *I*–*L* characteristics of the hybrid GaInAsP/SOI ridge waveguide FP laser with a cavity length of 2.0 mm under CW operation at elevated stage temperatures. The figure shows that lasing operation was demonstrated with stage temperatures up to 110 °C. Note that the actual temperature of the stage surface is slightly lower than the set value measured by a thermocouple inside the stage with an error of $<2\%$ (a few degrees). Wavelength dependences on temperature ($d\lambda/dT$) and injected power ($d\lambda/dP$) were measured to extract the thermal resistance ($Z_T = dT/dP$) from the equation $dT/dP = (d\lambda/dP)/(d\lambda/dT)$. Figures 7(a) and 7(b) show shifting of the FP lasing spectra with dissipated power and stage temperature, respectively, for the 2.0 mm cavity length. The extracted characteristic temperatures were $T_0 = 64$ K (from 20 °C to 60 °C) and $T_1 = 130$ K (from 20 °C to 40 °C). A thermal resistance of 14.3 K W^{-1} was extracted for the 2.0 mm cavity length. Additionally, a thermal resistance of 27.2 K W^{-1} was extracted for a 1.0 mm cavity length. This corresponds to almost double the extracted value for a 2.0 mm cavity length, which agrees well with the theory, as the thermal resistance is inversely proportional to the volume of the active region.

In conclusion, hybrid GaInAsP/SOI ridge waveguide FP lasers with improved thermal resistance were fabricated through SAB at room temperature. A ridge insulation structure with thin vertical cladding was introduced with a theoretical and experimental reduction in thermal resistance of 9.3% and 16.3%, respectively. By introducing the thermal shunt structure and Au electroplating in addition to the proposed ridge insulation structure, single-facet output power values of 12.5 mW and 20.0 mW with current threshold values of 18 mA and 48 mA was achieved under CW conditions for cavity lengths of 0.5 mm and 2.0 mm, respectively. The lasing operation was demonstrated with stage temperatures up to 110 °C for a cavity length of 2.0 mm. The proposed structure showed thermal resistance of 14.3 K W^{-1}

 © 2023 The Japan Society of Applied Physics

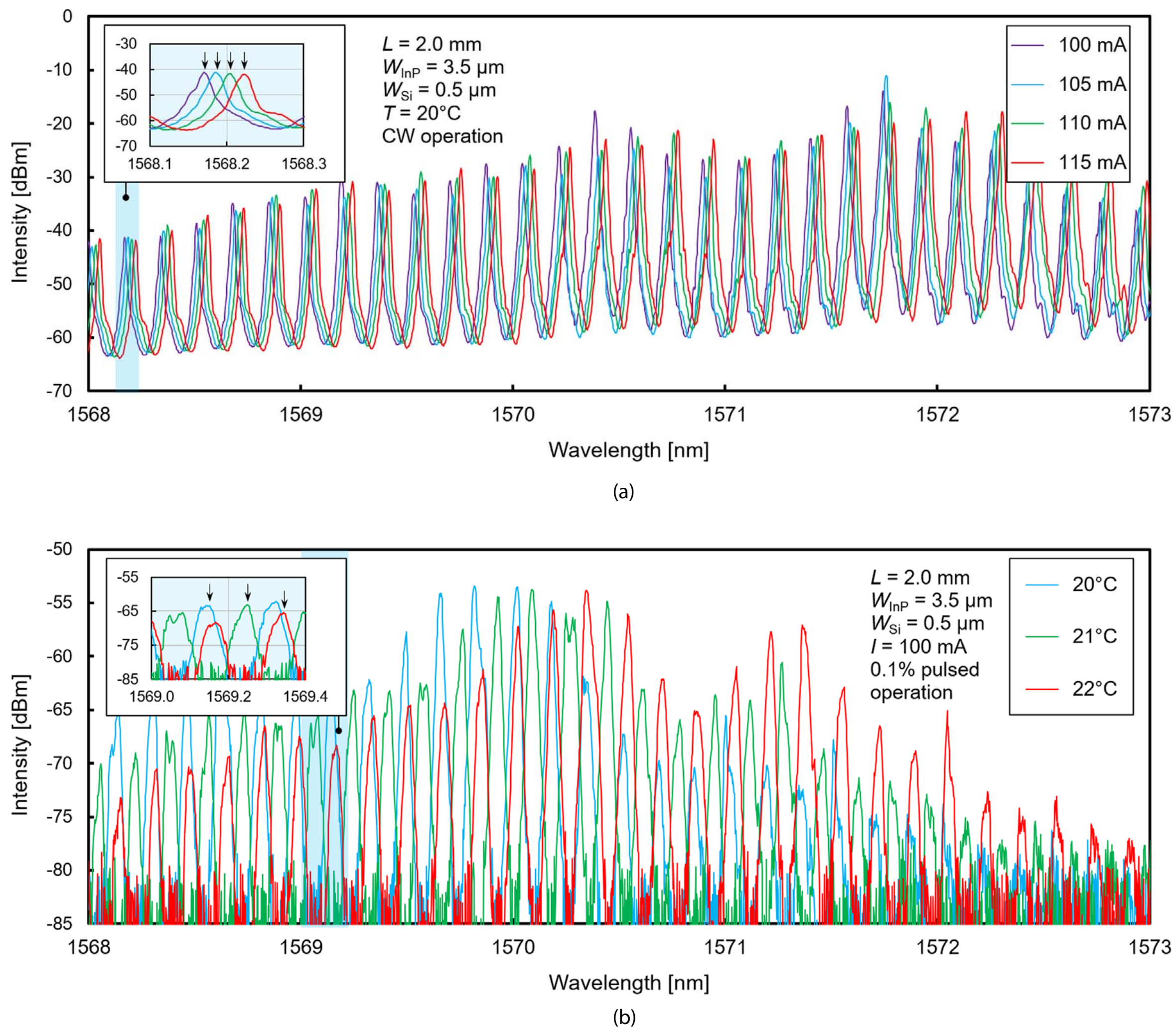

Fig. 7. (Color online) Lasing spectra shift of the hybrid GaInAsP/SOI FP ridge waveguide laser with (a) dissipated power (CW operation) and (b) stage temperature (pulsed operation).

and a threshold current density of ~0.7 kA cm^{-2} for the hybrid GaInAsP/SOI laser with a 2.0 mm cavity length.

Acknowledgments The authors would like to thank Takuo Hiratani, Naoko Inoue, Naoki Fujiwara, Toshiyuki Nitta and Hideki Yagi of Sumitomo Electric Industries for their fruitful discussions. This work was supported by New Energy and Industrial Technology Development Organization (NEDO) grant no. JPNP16007.

ORCID iDs Nobuhiko Nishiyama https://orcid.org/0000-0001-8288-6690

1) D. Liang, G. Roelkens, R. Baets, and J. E. Bowers, MDPI **3**, 1782 (2010).
2) M. J. Heck, J. F. Bauters, M. L. Davenport, J. K. Doylend, S. Jain, G. Kurczveil, S. Srinivasan, Y. Tang, and J. E. Bowers, IEEE J. Sel. Top. Quantum Electron. **19**, 6100117 (2012).
3) J. E. Bowers, T. Komljenovic, M. Davenport, J. Hulme, A. Y. Liu, C. T. Santis, A. Spott, S. Srinivasan, E. J. Stanton, and C. Zhang, Proc. SPIE **9774**, 977402 (2016).
4) S. Fathpour, IEEE J. Quantum Electron. **54**, 6300716 (2018).
5) P. Kaur, A. Boes, G. Ren, T. G. Nguyen, G. Roelkens, and A. Mitchell, APL Photonics **6**, 061102 (2021).
6) C. Xiang et al., IEEE J. Sel. Top. Quantum Electron. **28**, 8200515 (2021).
7) T. Komljenovic, D. Huang, P. Pintus, M. A. Tran, M. L. Davenport, and J. E. Bowers, Proc. IEEE **106**, 2246 (2018).
8) H. Guan et al., Opt. Express **26**, 7920 (2018).
9) S. Keyvaninia et al., Opt. Express **21**, 3784 (2013).
10) J. Hulme, J. Doylend, and J. Bowers, Opt. Express **21**, 19718 (2013).
11) T. Creazzo et al., Opt. Express **21**, 28048 (2013).
12) T. Mitarai, E. Moataz, T. Miyazaki, T. Amemiya, and N. Nishiyama, J. Appl. Phys. **59**, 112002 (2020).
13) D. Liang, M. Fiorentino, T. Okumura, H.-H. Chang, D. T. Spencer, Y.-H. Kuo, A. W. Fang, D. Dai, R. G. Beausoleil, and J. E. Bowers, Opt. Express **17**, 20355 (2009).
14) D. Liang, M. Fiorentino, S. Srinivasan, S. Todd, G. Kurczveil, J. Bowers, and R. Beausoleil, IEEE Photonics J. **3**, 580 (2011).
15) C. Zhang, D. Liang, G. Kurczveil, J. E. Bowers, and R. G. Beausoleil, IEEE J. Sel. Top. Quantum Electron. **21**, 385 (2015).
16) C. Zhang, G. K. Di Liang, and R. G. Beausoleil, Optica **6**, 1145 (2019).
17) M. N. Sysak, H. Park, A. W. Fang, J. E. Bowers, R. Jones, O. Cohen, O. Raday, and M. Paniccia, Opt. Express **15**, 15041 (2007).
18) H. Park, A. W. Fang, O. Cohen, R. Jones, M. J. Paniccia, and J. E. Bowers, IEEE Photonics Technol. Lett. **19**, 230 (2007).
19) M. N. Sysak, D. Liang, R. Jones, G. Kurczveil, M. Piels, M. Fiorentino, R. G. Beausoleil, and J. E. Bowers, IEEE J. Sel. Top. Quantum Electron. **17**, 1490 (2011).
20) Y. Hayashi, J. Suzuki, S. Inoue, S. M. T. Hasan, Y. Kuno, K. Itoh, T. Amemiya, N. Nishiyama, and S. Arai, J. Appl. Phys. **55**, 082701 (2016).
21) J. Suzuki, Y. Hayashi, S. Inoue, T. Amemiya, N. Nishiyama, and S. Arai, J. Appl. Phys. **56**, 062103 (2017).
22) D. Liang, S. Srinivasan, M. Fiorentino, G. Kurczveil, J. E. Bowers, and R. G. Beausoleil, Optical Interconnects Conf. **2012**, 50 (2012).
23) C. Zhang, D. Liang, G. Kurczveil, J. E. Bowers, and R. G. Beausoleil, Conf. on Lasers and Electro-Optics (CLEO) **2015**, 1 (2015).
24) M. N. Sysak, H. Park, A. Fang, O. Raday, J. E. Bowers, and R. Jones, Optical Fiber Communication Conf. **1**, OWZ6 (2011).

© 2023 The Japan Society of Applied Physics

25) Y. Wang, K. Nagasaka, T. Mitarai, Y. Ohiso, T. Amemiya, and N. Nishiyama, Jpn. J. Appl. Phys. **59**, 052004 (2020).
26) T. Kikuchi et al., Jpn. J. Appl. Phys. **61**, 052002 (2022).
27) M. Wang, T. Hosoda, L. Shterengas, G. Kipshidze, M. Lu, A. Stein, and G. Belenky, Opt. Eng. **57**, 011012 (2017).
28) Z.-K. Zhang, F. Xu, J.-C. Zhang, Z.-R. Lv, X.-G. Yang, and T. Yang, IEEE J. Quantum Electron. **54**, 1 (2018).
29) J. Xu, S. Liang, Z. Zhang, J. An, H. Zhu, and W. Wang, Opt. Laser Technol. **91**, 46 (2017).
30) Z. Lu et al., J. Eur. Opt. Soc. **17**, 9 (2021).
31) L. A. Coldren and S. W. Corzine, *Diode Lasers and Photonic Integrated Circuits* (Wiley, New York, 1995) 1st ed.
32) M. Eissa, T. Mitarai, T. Amemiya, Y. Miyamoto, and N. Nishiyama, Jpn. J. Appl. Phys. **59**, 126502 (2020).

© 2023 The Japan Society of Applied Physics